ACS Chemical Neuroscience

Research Article

pubs.acs.org/chemneuro

Binding of the Multimodal Antidepressant Drug Vortioxetine to the Human Serotonin Transporter

Jacob Andersen,[†] Lucy Kate Ladefoged,[‡] Danyang Wang,[†] Trine N. Bjerre Kristensen,[‡] Benny Bang-Andersen,[†,§] Anders S. Kristensen,[†] Birgit Schiøtt,[*,‡] and Kristian Strømgaard[*,†]

[†]Department of Drug Design and Pharmacology, University of Copenhagen, Universitetsparken 2, DK-2100 Copenhagen, Denmark

[‡]Center for Insoluble Protein Structures (inSPIN) and Interdisciplinary Nanoscience Center (iNANO), Department of Chemistry, Aarhus University, Langelandsgade 140, DK-8000 Aarhus C, Denmark

[§]Lundbeck Research Denmark, H. Lundbeck A/S, Ottiliavej 9, DK-2500 Valby, Denmark

Supporting Information

ABSTRACT: Selective inhibitors of the human serotonin transporter (hSERT) have been first-line treatment against depression for several decades. Recently, vortioxetine was approved as a new therapeutic option for the treatment of depression. Vortioxetine represents a new class of antidepressant drugs with a multimodal pharmacological profile that in addition to potent inhibition of hSERT include agonistic or antagonistic effects at different serotonin receptors. We used a combination of computational, chemical, and biological methods to decipher the molecular basis for high affinity binding of vortioxetine in hSERT. X-ray crystal structures of the bacterial amino acid transporter LeuT and the *Drosophila melanogaster* dopamine transporter were used to build homology models of hSERT. Comparative modeling and ligand docking suggest that vortioxetine can adopt several distinct binding modes within the central binding site of hSERT. To distinguish between the identified binding modes, we determined the effect of 57 functional hSERT point mutants on vortioxetine potency and characterized seven structurally related analogs of vortioxetine in a subset of the point mutants. This allowed us to determine the orientation of vortioxetine within the central binding site and showed that only one of the proposed binding modes is functionally relevant. The findings provide important new insight about the molecular basis for high affinity recognition of vortioxetine in hSERT, which is essential for future structure-based drug discovery of novel multimodal drugs with fine-tuned selectivity across different transporter and receptor proteins in the human brain.

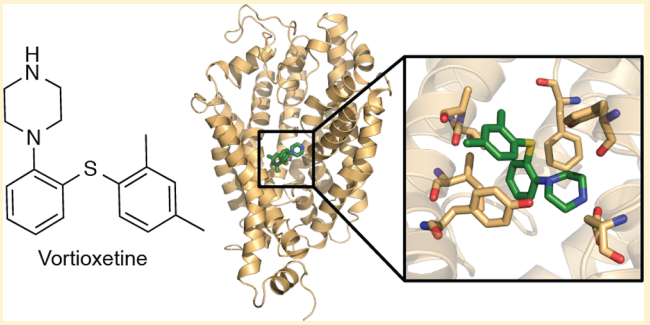

KEYWORDS: *serotonin transporter, antidepressant drug, neurotransmitter transport, induced fit docking, pharmacology, structure-based drug design*

The human serotonin transporter (hSERT) is an integral membrane protein that facilitates sodium- and chloride-dependent reuptake of released serotonin (5-hydroxytryptamine; 5-HT) into presynaptic neurons and thus plays a key role in synaptic 5-HT homeostasis and signaling.[1] 5-HT is involved in the modulation of a variety of behaviors, including mood, sleep, pain, appetite, aggression, and sexual activity, and pharmacological inhibition of hSERT is widely used in the treatment of a variety of psychiatric disorders, such as depression, anxiety, and obsessive-compulsive disorder.[2] In addition, psychostimulant drugs, such as amphetamine and 3,4-methylenedioxymethamphetamine (also known as ecstasy), also have hSERT among their molecular targets.[3]

The pharmacological principle behind the vast majority of today's antidepressants is to modulate serotonergic activity in the central nervous system, which descends from serendipitous observations in the 1950s, where it was realized that the tricyclic antidepressant drug imipramine relieved symptoms of depression by blocking the reuptake of biogenic monoamines in the human brain.[4,5] This finding led to the development of multiple structurally related analogs of imipramine and later to compounds specifically targeting SERT with little or no affinity for other CNS targets, the so-called selective serotonin reuptake inhibitors (SSRIs). The first SSRIs reached the market in the 1980s, and they still remain first-line pharmacological treatment against depression.[6] In 2014, vortioxetine (Figure 1) was approved as a new therapeutic option for treatment of major depressive disorder.[7] The pharmacological profile of vortioxetine extends beyond selective 5-HT reuptake blockage, and vortioxetine mediates its pharmacological activities through potent inhibition of SERT, 5-HT_{1A} receptor agonism, and antagonism at 5-HT_{1D}, 5-HT_3, and 5-HT_7 receptors, as well as

Received: August 18, 2015
Accepted: September 21, 2015
Published: September 21, 2015

DOI: 10.1021/acschemneuro.5b00225
ACS Chem. Neurosci. 2015, 6, 1892−1900

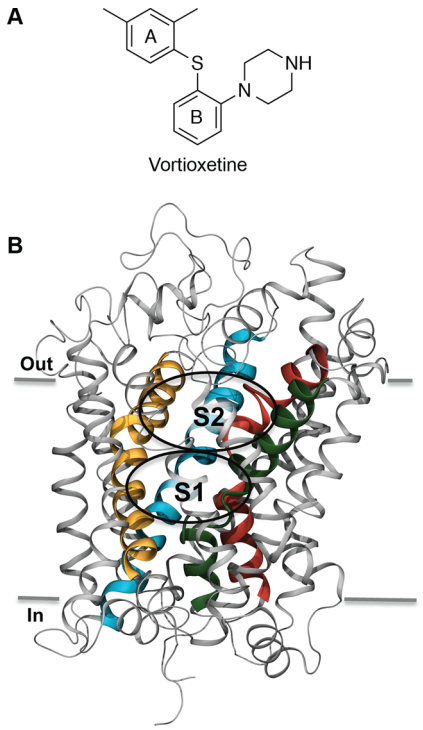

Figure 1. Structural overview of vortioxetine and SERT. (A) Structure of vortioxetine. The two phenyl rings are referred to as phenyl-A and phenyl-B, respectively. (B) Homology model of hSERT in an outward-facing open conformation ($SERT_{open}$) with the helices forming the S1 binding site shown in colors (TM1 in red, TM3 in yellow, TM6 in green, and TM8 in blue). The approximate location of the S1 and S2 binding sites, as well as the membrane spanning region of SERT, are indicated on the figure.

partial agonism at $5\text{-}HT_{1B}$ receptors.[8,9] In addition to its antidepressant activity, vortioxetine has recently showed positive effects on predefined cognition outcome measures in clinical studies.[10,11]

The hSERT belongs to the solute carrier 6 (SLC6) family of transporters, which also includes transporters for other neurotransmitters, including norepinephrine, dopamine, γ-aminobutyric acid, and glycine.[12] Given the clinical importance of hSERT, much research over the past decades has focused on deciphering the molecular details for how different drugs bind to hSERT. Direct structural information about hSERT in the form of X-ray crystal structures is still not available. However, the X-ray crystal structures of SLC6 transporter homologues, including the bacterial amino acid transporters LeuT and MhsT and the *Drosophila melanogaster* dopamine transporter (dDAT), have been determined.[13−18] These structures have provided important information about the location and structure of the ligand binding site as well as the substrate permeation pathway that can be extended to SLC6 transporters such as hSERT.[19−26] The X-ray crystal structures have revealed a protein structure with 12 transmembrane segments (TMs) connected by intra- and extracellular loop regions. The substrate binding site (denoted the S1 site) is formed by residues in TM1, 3, 6, and 8, and is located in the core of the transporter protein (Figure 1).[16,18,27] Although X-ray crystal structures of LeuT have shown that some antidepressant drugs bind to a site at an extracellular facing vestibule (denoted the S2 site),[28−30] structures of dDAT and LeuBAT (a LeuT/hSERT hybrid) have shown that the binding site for antidepressants and illicit drugs overlaps with the central S1 site.[15−17,31] Combined with mutational studies of hSERT showing that several S1 residues are critically important for the binding of antidepressants to the human transporter,[32−35] this provides compelling evidence that the high-affinity binding site for antidepressants is located within the S1 site in hSERT.

Vortioxetine represents a new class of antidepressant drugs, and very little is known about the binding of this novel multimodal drug to SERT. Here, we used a combination of computational, chemical, and biological approaches to decipher the molecular basis for binding of vortioxetine to hSERT. X-ray crystal structures of dDAT and LeuT were used to create homology models of hSERT in two different conformational states, followed by induced fit docking (IFD) of vortioxetine. The proposed binding modes were challenged by a mutational data set from >50 point mutants describing the contribution of residues in the S1 and S2 binding pockets to vortioxetine inhibition. Characterization of structurally related analogs of vortioxetine at selected point mutants provided further support for interactions between specific residues and structural motifs of the vortioxetine molecule, showing that only one of the five proposed binding modes is functionally relevant.

RESULTS AND DISCUSSION

Molecular Modeling of the Vortioxetine Binding Site in SERT. Homology models of hSERT were created for multiple conformational states to allow a more robust binding mode prediction through IFD. It is not known which conformational state vortioxetine stabilizes, and models of hSERT in an outward-facing occluded conformation ($SERT_{occ}$) and an outward-facing open conformation ($SERT_{open}$) were therefore constructed. The homology model of $SERT_{occ}$ was based on the substrate-bound LeuT X-ray crystal structure (PDB entry 2A65) as described previously,[36] and the model of $SERT_{open}$ was based on the nortriptyline-bound dDAT structure (PDB entry 4M48). The primary sequence of hSERT (Uniprot ID P31645) was aligned to dDAT using the AlignMe,[37−39] 2dalign, and salign[40] algorithms. The three alignments only differed with regard to seven residues, which were modeled as an insertion (Supporting Figure S1, Supporting Methods). Using MODELLER,[41−44] 20 homology models of $SERT_{open}$ were built and evaluated using several scoring functions and available biochemical data (Supporting Table S1, Supporting Methods), and the best model was subjected to loop optimization of a ten residue segment in EL2 that spans over the two insertion solutions, as well as an extra residue at both ends. Importantly, the best model of $SERT_{open}$ could reproduce the previously validated binding mode of 5-HT[21] in a docking study (Supporting Methods), and the overall conformation of $SERT_{open}$ remained stable in the outward open conformation during three 100 ns molecular dynamics simulations (Supporting Methods). The two hSERT models, $SERT_{open}$ and $SERT_{occ}$, differ in the size and accessibility of the S1 site. In $SERT_{open}$ the extracellular gate is open and together the S1 and S2 sites forms a funnel into the center of the transporter, while the two sites are clearly separated by the closed extracellular gate in $SERT_{occ}$. Furthermore, due to slight changes in the relative position between TM1, 3, 6, and 8, the S1 site is wider in $SERT_{open}$ allowing ligands to bind 1−2 Å further into the binding site toward the intracellular side.

To determine possible binding modes of vortioxetine in the S1 site of hSERT, an IFD calculation was performed for both models of hSERT (Supporting Methods). Furthermore,

DOI: 10.1021/acschemneuro.5b00225
ACS Chem. Neurosci. 2015, 6, 1892−1900

Table 1. Results from the Induced Fit Docking (IFD) Calculations of Vortioxetine into the S1 Site of $SERT_{open}$ and $SERT_{occ}$ Models[a]

cluster	poses	avg Emodel	avg Gscore	avg IFDscore
		$SERT_{open}$		
$C1_{open}$	9	−57.6 ± 5.9	−7.8 ± 0.4	−1100.5 ± 0.4
$C2_{open}$	11	−60.6 ± 5.3	−8.1 ± 0.4	−1101.1 ± 0.6
$C3_{open}$	19	−59.6 ± 3.8	−8.1 ± 0.5	−1100.9 ± 0.5
$C4_{open}$	40	−61.2 ± 6.5	−9.1 ± 0.4	−1102.1 ± 0.6
$C5_{open}$	11	−56.2 ± 6.9	−8.0 ± 0.6	−1100.9 ± 0.8
Outliers	3			
		$SERT_{occ}$		
$C1_{occ}$	7	−42.6 ± 14	−9.8 ± 0.8	−1086.5 ± 0.6
$C2_{occ}$	7	−35.3 ± 21	−10.1 ± 0.6	−1086.8 ± 0.9
$C3_{occ}$	2	−52.3 ± 14	−11.2 ± 0.2	−1087.9 ± 0.0
$C4_{occ}$	6	−43.3 ± 22	−9.6 ± 0.3	−1086.2 ± 0.4
Outliers	4			

[a]Average Emodel, Gscore, and IFD scores (kcal/mol) are reported for each cluster with accompanying standard deviations. Number of outliers is also reported.

docking was also attempted in the S2 site of the $SERT_{occ}$ model. Five main clusters, $C1-5_{open}$, with similar binding scores were found when docking vortioxetine into the S1 site of $SERT_{open}$ (Table 1, Supporting Table S2). In all five clusters, the piperazine ring of vortioxetine is located at subsite A[19,35] (see Figure 2A for subsite definitions) of the binding pocket close to Tyr95 and Asp98. The secondary amine of the piperazine ring is interacting with the carboxylate group of Asp98 plus the backbone carbonyl oxygen atoms of Tyr95 ($C2_{open}$ and $C5_{open}$), Phe335 ($C2_{open}$), or Ser336 ($C1_{open}$ and $C3_{open}$) in addition to forming cation-π interactions with Tyr95. Both $C1_{open}$ and $C2_{open}$ display interactions between the dimethylphenyl ring of vortioxetine (referred to as phenyl-A; see Figure 1) and subsite B, while the central phenyl ring of vortioxetine (referred to as phenyl-B; see Figure 1) interacts with subsite C (Figure 2B,C). $C1_{open}$ and $C2_{open}$ are distinguished by a shift of the phenyl rings by approximately 3 Å allowing phenyl-A to engage in π-stacking with Tyr176 in $C1_{open}$ but not in $C2_{open}$. Differences are also observed in the interactions between phenyl-B and residues in subsite C. Specifically, phenyl-B interacts with Tyr95, Ala169, and Ile172 in $C1_{open}$, but with Tyr95, Ile172, Phe335, and Phe341 in $C2_{open}$. The shift of the phenyl rings within the binding site allows the sulfur atom of vortioxetine to form a weak hydrogen bond to Tyr95 in $C2_{open}$ but not in $C1_{open}$. The remaining three clusters, $C3-5_{open}$, display vortioxetine in a reverse orientation with regards to the phenyl rings; that is, phenyl-A interacts with subsite C, while phenyl-B interacts with subsite B. The three clusters differ by shifts in the position of the phenyl groups within the binding site (Figure 2D−F). In $C3_{open}$, phenyl-A makes hydrophobic interactions with Tyr95, Ile168, Ala169, Ile172, and Val343 in subsite B and is thus positioned slightly deeper into the binding site than in the other clusters (Figure 2D), while phenyl-B of vortioxetine interacts with Ile172 and Tyr176 in subsite B and is otherwise facing the extracellular solvent. Phenyl-A reaches even further into the S1 site in $C4_{open}$ and makes hydrophobic interactions with Ile165, Ile168, Ala169, Ile172, Phe341, Val343, and Val501, whereas the phenyl-B ring interacts with Ala169, Ile172, Ala173, and Tyr176. A few poses in $C4_{open}$ and $C5_{open}$ also display hydrogen bonding between the sulfur atom of vortioxetine and Tyr95. In $C5_{open}$, phenyl-A of vortioxetine is positioned between Ile168, Ile172, and Thr497 and also interacts with Ala169 and Phe341, while phenyl-B interacts with Tyr95 through π-stacking, and Ala169, Ile172, Tyr176, and Val343 through hydrophobic interactions.

Docking of vortioxetine into the S1 site of $SERT_{occ}$ resulted in four clusters ($C1-4_{occ}$) (Table 1; Supporting Table S2). Two clusters, $C1-2_{occ}$, represent the same binding modes as found in $C1-2_{open}$, respectively (Supporting Figure S2), while the binding mode of vortioxetine in $C3-4_{occ}$ was similar to the

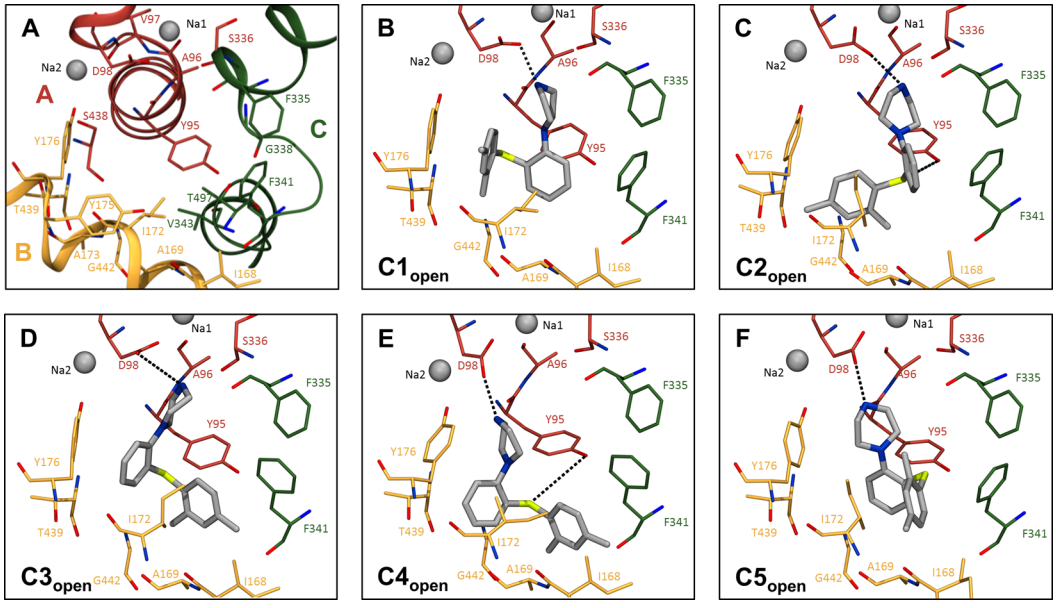

Figure 2. Representative binding modes of vortioxetine within the S1 site of $hSERT_{open}$. (A) The subsite definitions of the S1 site are colored based on the primary helix within the subsite: TM1 = subsite A (red), TM3 = subsite B (yellow), and TM6 = subsite C (green). Residues on TM8 are shared between subsite A and B. (B−F) A representative pose from each cluster in $SERT_{open}$ ($C1-5_{open}$) is shown, and potential hydrogen bonds between vortioxetine and S1 residues are shown as broken black lines.

DOI: 10.1021/acschemneuro.5b00225
ACS Chem. Neurosci. 2015, 6, 1892−1900

binding modes observed in C3−5_{open}. However, the secondary amine of vortioxetine interacted with the backbone carbonyl of Phe335 or Ser336 in C3−4_{occ} rather than Asp98, as observed in C3−5_{open}. Two clusters, $C2_{occ}$ and $C4_{occ}$, display hydrogen bonding between the vortioxetine sulfur atom and Tyr95 in a subset of poses. Overall, IFD of vortioxetine into the central site in $SERT_{open}$ and $SERT_{occ}$ yielded strikingly similar binding clusters, indicating that these likely represent important binding modes of vortioxetine that can exist in several conformations of hSERT. For simplicity, we will use the binding clusters derived from IFD into $SERT_{open}$ (C1−5_{open}) as representatives for the binding clusters obtained from IFD into both $SERT_{open}$ and $SERT_{occ}$ and discuss our mutational data (*vide infra*) in relation to these clusters.

Vortioxetine was also docked into S2 of $SERT_{occ}$, which resulted in multiple binding poses with binding scores similar to those observed from docking vortioxetine at S1 (Supporting Table S2). The poses could be grouped into three clusters in which the secondary amine of vortioxetine forms a salt bridge with Glu493 in all clusters. However, the orientation of the aromatic rings was not well-defined, and no other strong interactions between vortioxetine and hSERT were found (Supporting Figure S3). An IFD of vortioxetine into the S2 site of $SERT_{open}$ was not attempted due to the larger volume of the S2 site in this model compared with the S2 site in $SERT_{occ}$.

Mutational Mapping of the Vortioxetine Binding Site. To distinguish between the binding clusters of vortioxetine obtained from IFD calculations, we performed a mutational analysis of residues located in the S1 and S2 binding regions of hSERT. Specifically, we included 67 point mutations across 23 different positions in the S1 and S2 sites of hSERT (Figure 3; Supporting Table S4). Initially, the hSERT mutants were expressed in COS-7 cells and assayed for functionality in a [^{3}H]5-HT uptake assay (Supporting Methods). We determined the inhibitory potency (K_i) of vortioxetine at the 57 functional mutants in a [^{3}H]5-HT uptake inhibition assay (Figure 3). At six positions (Tyr95, Ile168, Ala169, Ile172, Phe341, and Gly442), point mutations induced >5-fold shifts in the K_i-value for vortioxetine (ranging from 5−26-fold), suggesting that these residues play an important role in vortioxetine binding. The six important residues are located in all three subsites of the S1 pocket (Tyr95 in subsite A; Ile168, Ala169, Ile172, and Gly442 in subsite B; Phe341 in subsite C), and the results thus immediately suggest that (i) vortioxetine binds within the central S1 binding site and (ii) high-affinity binding of vortioxetine is dependent on interactions at all three subsites of the S1 binding pocket.

The six residues that were identified as key determinants for vortioxetine binding are located within 5 Å of vortioxetine in all five S1 binding clusters (C1−5_{open}), substantiating the hypothesis that one of the predicted clusters represents the bioactive binding mode of vortioxetine in hSERT. Previous studies have shown that Tyr95 has an important role for binding of antidepressants in hSERT.[20,24,34,35,45,46] Tyr95 is located between the piperazine ring and one of the phenyl rings of vortioxetine in C1−5_{open}, and Tyr95 can thus form hydrophobic interactions and cation-π interactions with these moieties. Removal of the aromatic ring of Tyr95 (Y95A and Y95V) induced a 9−26-fold loss of potency for vortioxetine, which supports the idea that the side chain of Tyr95 interacts directly with vortioxetine. When substituting Tyr95 with tryptophan (Y95W), we observed a 2-fold decrease in the potency of vortioxetine, which could be due to a steric clash from the larger tryptophan compared with tyrosine. Interestingly, Y95F did not significantly affect the potency of

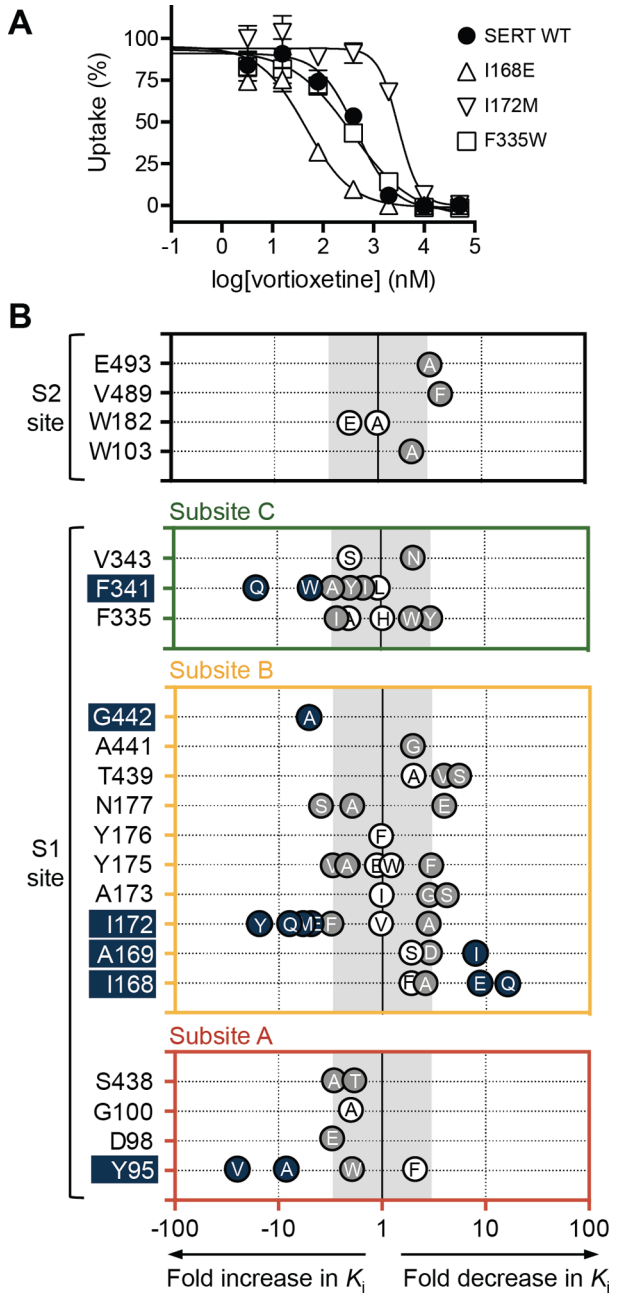

Figure 3. Effect of point mutations in the S1 and S2 sites of hSERT on vortioxetine potency. (A) Representative dose−response curves from a [^{3}H]5-HT uptake inhibition assay with vortioxetine. Data points represent mean ± SEM from triplicate determinations. (B) Graphic summary of the fold-change in K_i of vortioxetine induced by introduction of point mutations in subsites A, B, and C and in the S2 site. Data represent mean fold-change from at least three independent experiments, in which WT and mutant were assayed in parallel. The fold-change was calculated as K_i(WT)/K_i(mutant) or −K_i(mutant)/K_i(WT) for mutations increasing or decreasing vortioxetine potency, respectively. The gray shaded region indicates <3-fold changes in vortioxetine potency. Gray and blue shading of data points specify that the mutation induce a significant change in vortioxetine K_i ($p < 0.05$; paired Student's *t*-test). Mutations producing >5-fold change in vortioxetine potency and their corresponding positions are highlighted in blue.

DOI: 10.1021/acschemneuro.5b00225
ACS Chem. Neurosci. 2015, 6, 1892−1900

vortioxetine, suggesting that it is the aromaticity and not the hydroxyl group of Tyr95 that is interacting with vortioxetine. The sulfur atom in vortioxetine interacts directly with the side-chain hydroxyl group of Tyr95 in a small subset of the binding poses in $C2_{open}$ (3/11 poses), $C4_{open}$ (3/40 poses), and $C5_{open}$ (6/11 poses). Hence, the lack of an effect of the Y95F mutation on vortioxetine potency could indicate that $C2_{open}$, $C4_{open}$, and $C5_{open}$ do not represent bioactive binding modes of vortioxetine in hSERT.

Ile168 and Ala169 are located in the lower part of the S1 binding site close to one of the phenyl rings of vortioxetine in $C1-5_{open}$ (Figure 2B–F). Introduction of polar or charged residues into these positions (I168E, I168Q, A169D) significantly decreased the K_i of vortioxetine, showing that increasing the polarity in this part of the binding pocket had a positive impact on vortioxetine binding. However, the increased polarity does not complement the nonpolar phenyl groups of vortioxetine, suggesting that the effect of the polar mutations may be through indirect interactions. Adding more bulk to the Ala169 side chain (A169I) also induced a significant increase (8-fold) in vortioxetine potency, which could be induced by increased hydrophobic interactions with one of the phenyl rings of vortioxetine.

In $C1-5_{open}$, the side-chain of Ile172 is sandwiched between phenyl-A and phenyl-B of vortioxetine (Figure 2B–F), suggesting that Ile172 is important for vortioxetine binding. Accordingly, we found that mutation of Ile172 to glutamate, methionine, phenylalanine, glutamine, or tyrosine led to loss of potency for vortioxetine (3–14-fold), thereby corroborating earlier findings that Ile172 is critical for high affinity inhibitor binding to hSERT.[34,35,47]

Phe341 is located close to one of the phenyl rings of vortioxetine in all five binding clusters (Figure 2B–F). Mutation of Phe341 to alanine, isoleucine, leucine, tryptophan, or tyrosine induced <5-fold changes in vortioxetine K_i, whereas F341Q induced a significant 16-fold loss of potency for vortioxetine, probably because this mutation does not complement interactions with the hydrophobic phenyl rings of vortioxetine.

Taken together, the lack of an effect from the Y95F mutation on vortioxetine potency suggests that $C2_{open}$, $C4_{open}$, and $C5_{open}$ do not represent the bioactive binding mode of vortioxetine in SERT, whereas it seems difficult to distinguish between $C1-5_{open}$ based on the mutational data obtained for the other identified key positions. However, since it is only a subset of the poses in $C2_{open}$, $C4_{open}$, and $C5_{open}$ that have been observed to form a hydrogen bond to Tyr95, these clusters cannot be disregarded solely based on the Y95F mutant. We were therefore unable to establish the functionally relevant binding mode of vortioxetine in hSERT based on the initial mutational analysis of binding site residues, and further experiments were thus required to establish the bioactive orientation of vortioxetine within the S1 site in hSERT.

Prediction of the Functionally Relevant Binding Mode of Vortioxetine in SERT. The binding poses of vortioxetine in $C1-2_{open}$ and $C3-5_{open}$ are almost mirror images of each other. In $C1-2_{open}$, phenyl-A of vortioxetine is binding in subsite B, and phenyl-B in subsite C, while phenyl-B is located in subsite B and phenyl-A ring in subsite C in $C3-5_{open}$. To establish the functionally relevant binding mode of vortioxetine in hSERT, we sought to identify which of the phenyl rings in vortioxetine interacts with residues in subsites B and C. Specifically, we determined the inhibitory potency of seven structurally related

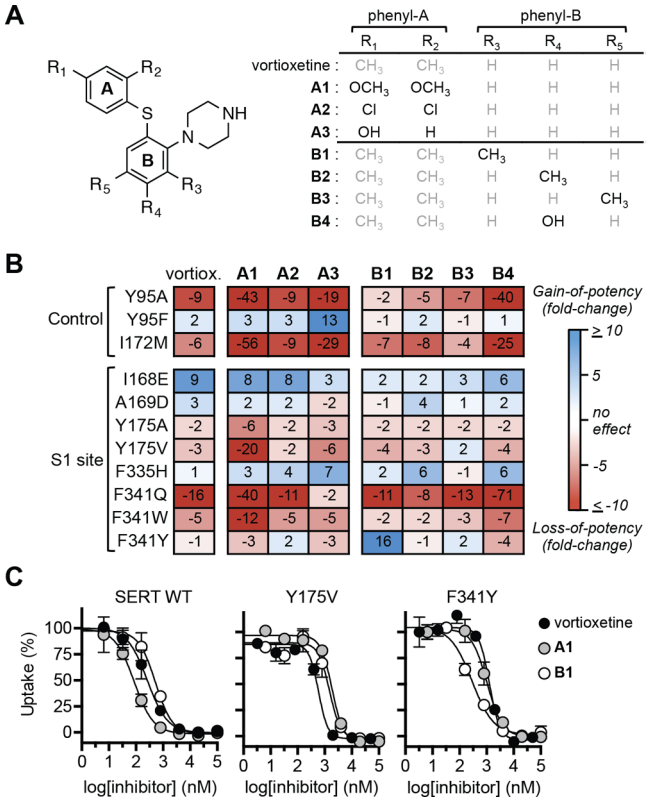

Figure 4. Effect of point mutations in the S1 site on vortioxetine analogs. (A) Structure of vortioxetine and the seven structurally related analogs. (B) Heat-map representation of mutation-induced changes in the potency of vortioxetine and analogs carrying modifications on phenyl-A (**A1**–**A3**) or phenyl-B (**B1**–**B4**). The fold-changes was calculated as $K_i(WT)/K_i(mutant)$ or $-K_i(mutant)/K_i(WT)$ for mutations increasing or decreasing inhibitory potency, respectively, from experiments in which WT and mutant were assayed in parallel. Data represent mean fold-change calculated from at least three independent experiments. (C) Representative dose–response curves from [^{3}H]5-HT uptake inhibition experiments for vortioxetine (black circles), **A1** (gray circles), and **B1** (open circles) at WT (left), Y175V (middle), and F341Y (right). Data points represent mean ± SEM from triplicate determinations.

analogs of vortioxetine at 12 point mutants of hSERT (Supporting Table S5), and the fold-change in K_i compared with WT was plotted as a heat map (Figure 4). The analogs included three compounds with different substituents on phenyl-A (**A1**–**A3**) and four compounds with different substituents on phenyl-B (**B1**–**B4**) compared with vortioxetine (Figure 4). Our hypothesis was, that if an analog is differentially affected by a mutation compared with vortioxetine, it indicates that the modified part of vortioxetine is located close to the mutated residue. In contrast, if the mutated residue is located distantly from the modified part of vortioxetine, the mutation would affect vortioxetine and the analog to a similar extent. This approach relies on the assumption that all analogs assume a similar binding mode as vortioxetine in hSERT. To verify this assumption, we used Y95A, Y95F, and I172M as controls. Tyr95 and Ile172 interact similarly with vortioxetine in $C1-5_{open}$, and if the analogs obtain a similar binding pose as vortioxetine, we expected them to be similarly affected by the Tyr95 and Ile172 mutants as vortioxetine. **A2**, **B2**, and **B3** were affected to a similar extent as vortioxetine by Y95A, Y95F, and I172M, suggesting that these compounds bind similarly as

DOI: 10.1021/acschemneuro.5b00225
ACS Chem. Neurosci. 2015, 6, 1892–1900

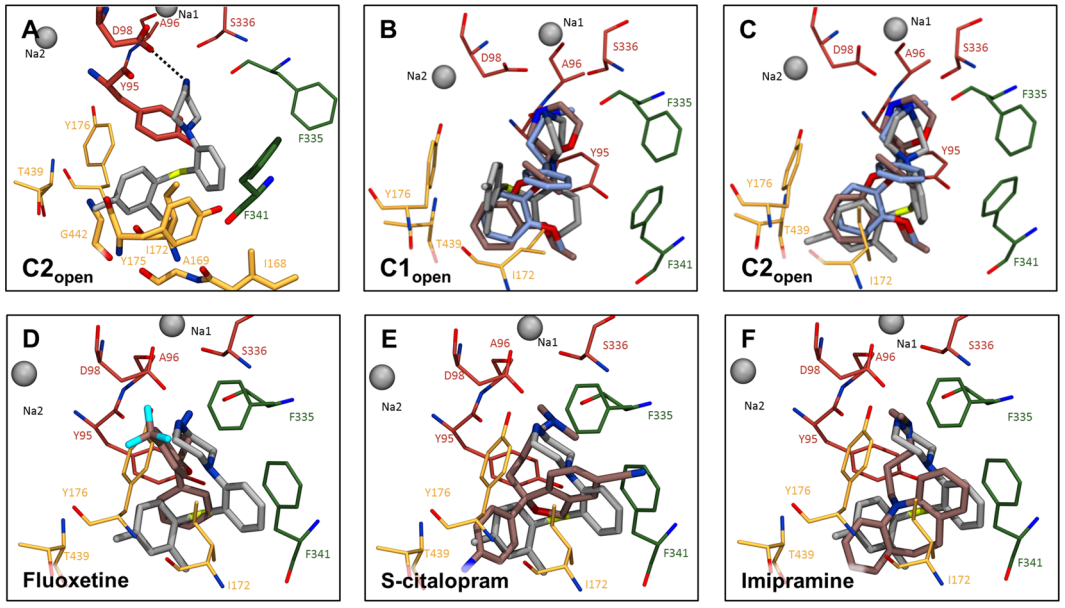

Figure 5. Comparison of the functionally relevant binding mode of vortioxetine in hSERT with binding modes of other inhibitors. (A) Vortioxetine ($C2_{open}$) is shown with the key interaction partners highlighted. (B–C) The binding mode of reboxetine (brown) and nisoxetine (blue) from dDAT X-ray crystal structures (PDB entry 4XNU and 4XNX, respectively) is overlaid with the binding mode of vortioxetine (gray) in $C1_{open}$ (B) and $C2_{open}$ (C). (D–F) The binding mode of vortioxetine (gray) in $C2_{occ}$ is overlaid with experimentally validated binding modes of fluoxetine[20] (D), *S*-citalopram[24] (E), and imipramine[25] (F) in hSERT.

vortioxetine (Figure 4). The potency of all analogs was decreased by Y95A and I172M, but the potency of **A1**, **A3**, and **B4** were more affected (19–56-fold loss of potency) compared with vortioxetine (6–9-fold loss of potency), and the potency of **B1** was less affected by Y95A compared with vortioxetine (2-fold versus 9-fold loss of potency). Furthermore, while Y95F did not significantly affect the potency of vortioxetine, the mutation induced a 13-fold gain of potency for **A3** (Figure 4). Since **A1**, **A3**, **B1**, and **B4** were differentially affected by Y95A, Y95F, or I172M compared with vortioxetine, we performed IFD of these four analogs into WT $SERT_{open}$ to verify whether they bind similarly as vortioxetine. IFD of **A3** in WT $SERT_{open}$ showed that **A3** interacts differently than vortioxetine in approximately two-thirds of the poses because the *para*-hydroxyl group of **A3** forms a hydrogen bond to Thr439 or backbone carbonyls in the vicinity (Supporting Figure S4). Furthermore, IFD of **B4** in WT $SERT_{open}$ showed that the hydroxyl group in **B4** is able to hydrogen bond to Asp98 or the backbone carbonyl of Ser438 leading to binding conformations that are not similar to vortioxetine in the majority of poses (Supporting Figure S4). It was thus concluded that **A3** and **B4** could not be used in determining the binding mode of vortioxetine. In contrast, IFD of **A1** and **B1** into WT $SERT_{open}$ showed that these analogs bind similarly as vortioxetine in the majority of the poses (46/54 and 20/28 poses, respectively), substantiating that these analogs could be used for distinguishing between the binding modes of vortioxetine (Supporting Figure S4).

We then focused on compounds **A1** and **A2**, in which the two methyl substituents on phenyl-A are substituted by methoxy groups (**A1**) or chloro atoms (**A2**) (Figure 4). Compared with vortioxetine, both compounds generally displayed similar sensitivity toward subsite C mutations. However, a different pattern was observed for Y175A and Y175V in subsite B, where inhibition of **A1** was more affected than vortioxetine. Specifically, Y175V induced a 20-fold loss of potency for **A1** compared with a 3-fold loss of potency for vortioxetine. This suggests that Tyr175 is located vicinal to phenyl-A of vortioxetine. IFD of **A1** into $SERT_{open}$ revealed that the methoxy group of **A1** can form a hydrogen bond to the side-chain hydroxyl group of Tyr175 and thus provides an explanation for the increased sensitivity of **A1** toward Tyr175 mutations compared with vortioxetine, which cannot engage in similar direct interactions with Tyr175 (Supporting Figure S4).

Next, we focused on analogs of vortioxetine in which phenyl-B was substituted with a methyl (**B1–B3**) (Figure 4). The majority of the mutations produced similar effects with these analogs as with vortioxetine. Interestingly, the I168E mutation induced a 9-fold gain of potency for vortioxetine, whereas the mutation only induced a 2–3-fold gain of potency for **B1**, **B2**, and **B3**. Since introduction of a negatively charged residue does not complement direct interactions with the aromatic phenyl rings of vortioxetine, it seems likely that the I168E mutation affects inhibitor binding indirectly by changing the size, shape, or electrostatic properties of the binding site cavity. However, these indirect effects are selectively affected by analogs modified around phenyl-B only, and the differential sensitivity toward I168E for **B1–B3** compared with vortioxetine, **A1**, and **A2** could indicate that phenyl-B of vortioxetine is vicinal to Ile168. Furthermore, F341Y selectively induced a 16-fold gain in the affinity of **B1**, whereas vortioxetine and the other analogs were not affected to the same extent (<4-fold change in K_i) (Figure 4). In an attempt to determine the reason for this increased affinity for **B1**, we performed IFD of **B1** in WT and F341Y $SERT_{open}$ models. When docking **B1** into WT $SERT_{open}$, we observed that **B1** binds similarly to vortioxetine in $C1–2_{open}$ and $C4_{open}$. Interestingly, when docking into the F341Y model, **B1** binds in a conformation very similar to $C2_{open}$ but with the phenyl-B ring moved approximately 2 Å closer to Phe335. According to the IFD calculations, this new conformation could be formed due to a hydrogen bond between F341Y and Thr497 that moves F341Y approximately 1.5 Å out of S1. This allows

DOI: 10.1021/acschemneuro.5b00225
ACS Chem. Neurosci. 2015, 6, 1892–1900

the methyl substituent of phenyl-B to make hydrophobic interactions with Phe335 (Supporting Figure S4). This would not be possible for **B2** and **B3** since the methyl substituent on phenyl-B for these two compounds would clash sterically with F341Y in its new position, and vortioxetine itself would not gain anything from this extra space. Together, these results suggest that phenyl-B of vortioxetine is binding in the vicinity of Ile168 and Phe341 in subsite C.

In summary, analysing the effect of 12 point mutations in hSERT on the potency of vortioxetine analogs allowed us to establish that phenyl-A of vortioxetine is in the vicinity of Tyr175 in subsite B and phenyl-B is oriented toward Ile168 and Phe341 in subsite C. These observations indicate that either $C1_{open}$ or $C2_{open}$ represents the bioactive orientation of vortioxetine in hSERT. It is noteworthy that G442A induced a significant 5-fold loss of potency for vortioxetine (Figure 3). The C-α atom of Gly442 is located approximately 1 Å closer to phenyl-A in $C2_{open}$ compared with $C1_{open}$, suggesting that the significant loss of potency by G442A could be induced by a steric clash in $C2_{open}$ but not in $C1_{open}$. Taken together, $C2_{open}$ is compatible with the majority of our experimental data, and we therefore suggest that $C2_{open}$ represents the bioactive binding mode of vortioxetine in hSERT.

Examination of the Predicted Binding Mode of Vortioxetine. We compared $C2_{open}$ to the available structure−activity relationship data for vortioxetine. It has been shown that a *para-tert*-butyl substituent on phenyl-A decreases hSERT activity, whereas the smaller CH_3, CF_3, and OCH_3 substituents on phenyl-A are well tolerated.[8] In $C2_{open}$, phenyl-A of vortioxetine is sandwiched between TM3 and TM8, thus explaining why larger substituents on this ring are not tolerated. In a subset of the poses in $C2_{open}$, the sulfur atom forms a hydrogen bond to Tyr95. Changing sulfur to oxygen would increase the strength of this hydrogen bond and thus improve binding to hSERT. However, substituting the sulfur for oxygen leads to loss of activity.[8] Together with the observation that the Y95F mutant did not affect the potency of vortioxetine (Figure 3), these data indicate that the putative hydrogen bond to Tyr95 is not critical for the high affinity binding of vortioxetine in hSERT.

Comparison of the proposed binding mode of vortioxetine in hSERT ($C2_{open}$) with structures of dDAT cocrystallized with nisoxetine and reboxetine revealed strikingly common features with vortioxetine (Figure 5C).[17] Specifically, an overlay of a representative pose of $C2_{open}$ onto the dDAT structures show that the phenyl rings of nisoxetine and reboxetine are sandwiched in between TM3 and TM8 similarly to the phenyl rings of vortioxetine in the $C2_{open}$ binding mode, but not in $C1_{open}$, further supporting the suggestion that $C2_{open}$ represents the bioactive binding mode (Figure 5B,C). Furthermore, a comparison between the binding mode of vortioxetine in $C2_{occ}$ with previously established binding models of fluoxetine,[20] (*S*)-citalopram,[24] and imipramine[25] in hSERT in an outward-facing occluded conformation ($SERT_{occ}$) showed that, although the binding site for all four inhibitors is overlapping the central S1 site, they obtain distinct binding modes within the binding cavity (Figure 5D−F). It is noteworthy that vortioxetine, (*S*)-citalopram, and imipramine are binding deep in the S1 site with aromatic moieties occupying both subsite B and C, while fluoxetine is binding higher up in the binding site with the CF_3 substituted phenyl ring extending toward the S2 site (Figure 5D−F). The distinct binding modes are consistent with experimental data showing that mutation of some residues (e.g., Tyr95 and Ile172) affect all four inhibitors, whereas mutation of other residues (e.g., Asp98, Phe341, and Ser438) selectively affect only some of the inhibitors (Figure 3).[35] Interestingly, the distinct binding modes of the four inhibitors indicate that it is possible to exploit different residues and regions within the S1 site to obtain high affinity binding in hSERT, which may be exploited in future design of hSERT inhibitors.

In summary, we have generated an experimentally validated model of the functionally relevant binding mode of vortioxetine in hSERT ($C2_{open}$) by combining comparative modeling with mutational analysis and characterization of drug analogs binding to selected point mutants. Recent X-ray crystal structures of mammalian 5-HT receptors[48−50] now also allow for construction of vortioxetine binding models in 5-HT receptors. Intriguingly, comparison of the vortioxetine model described herein with future models of vortioxetine binding in 5-HT receptors may provide a platform for designing novel multimodal drugs with tailor-made activity across several 5-HT proteins.

■ ASSOCIATED CONTENT

Supporting Information

The Supporting Information is available free of charge on the ACS Publications website at DOI: 10.1021/acschemneuro.5b00225. A pdb file of the validated binding mode of vortioxetine in hSERT ($C2_{open}$) in addition to the parameters of vortioxetine used in IFD calculations can be obtained from the authors.

Detailed descriptions of the methods used in this study, supporting figure S1−S4 showing the alignment used in homology modeling and illustrations of the binding modes of vortioxetine and vortioxetine analogs, and supporting tables S1−S5 providing homology modeling, IFD calculations, and uptake kinetics and inhibitor potencies from [^{3}H]5-HT uptake assays (PDF)

■ AUTHOR INFORMATION

Corresponding Authors

*Birgit Schiøtt. E-mail: birgit@chem.au.dk.

*Kristian Strømgaard. E-mail: kristian.stromgaard@sund.ku.dk.

Author Contributions

J.A. and L.K.L. contributed equally to this work. J.A., L.K.L., A.S.K., B.S., and K.S. designed research. J.A., L.K.L., D.W., and T.N.B.K. performed research. J.A., L.K.L., B.S., and K.S. analyzed data. B.B.-A. contributed new reagents and analytical tools. J.A., L.K.L., B.S., and K.S. wrote the manuscript with input from all authors.

Funding

We are grateful for financial support from the Carlsberg Foundation, the Lundbeck Foundation, the Danish National Research Foundation (DNRF59), and the Danish Council for Independent Research, Medical Sciences. Computations were made possible through allocations at the Center for Scientific Computing, Aarhus (CSC-Aa).

Notes

The authors declare the following competing financial interest(s): Benny Bang-Andersen is an employee of H. Lundbeck A/S. The other authors declare no competing financial interests.

DOI: 10.1021/acschemneuro.5b00225
ACS Chem. Neurosci. 2015, 6, 1892−1900

■ ACKNOWLEDGMENTS

The authors thank Dr. Julie Grouleff for fruitful discussions.

■ ABBREVIATIONS

5-HT, serotonin; dDAT, *Drosophila melanogaster* dopamine transporter; hSERT, human serotonin transporter; IFD, induced fit docking; SSRI, selective serotonin reuptake inhibitor; TM, transmembrane segment; WT, wild-type

■ REFERENCES

(1) Torres, G. E., Gainetdinov, R. R., and Caron, M. G. (2003) Plasma membrane monoamine transporters: structure, regulation and function. *Nat. Rev. Neurosci. 4*, 13−25.

(2) Kristensen, A. S., Andersen, J., Jørgensen, T. N., Sørensen, L., Eriksen, J., Loland, C. J., Strømgaard, K., and Gether, U. (2011) SLC6 neurotransmitter transporters: structure, function, and regulation. *Pharmacol. Rev. 63*, 585−640.

(3) Sitte, H. H., and Freissmuth, M. (2015) Amphetamines, new psychoactive drugs and the monoamine transporter cycle. *Trends Pharmacol. Sci. 36*, 41−50.

(4) Axelrod, J., Whitby, L. G., and Hertting, G. (1961) Effect of psychotropic drugs on the uptake of [^{3}H]-norepinephrine by tissues. *Science 133*, 383−384.

(5) Kuhn, R. (1958) The treatment of depressive states with G 22355 (imipramine hydrochloride). *Am. J. Psychiatry 115*, 459−464.

(6) Dale, E., Bang-Andersen, B., and Sanchez, C. (2015) Emerging mechanisms and treatments for depression beyond SSRIs and SNRIs. *Biochem. Pharmacol. 95*, 81−97.

(7) Zhang, J., Mathis, M. V., Sellers, J. W., Kordzakhia, G., Jackson, A. J., Dow, A., Yang, P., Fossom, L., Zhu, H., Patel, H., Unger, E. F., and Temple, R. J. (2015) The US Food and Drug Administration's perspective on the new antidepressant vortioxetine. *J. Clin. Psychiatry 76*, 8−14.

(8) Bang-Andersen, B., Ruhland, T., Jørgensen, M., Smith, G., Frederiksen, K., Jensen, K. G., Zhong, H., Nielsen, S. M., Hogg, S., Mørk, A., and Stensbøl, T. B. (2011) Discovery of 1-[2-(2,4-dimethylphenylsulfanyl)phenyl]piperazine (Lu AA21004): a novel multimodal compound for the treatment of major depressive disorder. *J. Med. Chem. 54*, 3206−3221.

(9) Sanchez, C., Asin, K. E., and Artigas, F. (2015) Vortioxetine, a novel antidepressant with multimodal activity: review of preclinical and clinical data. *Pharmacol. Ther. 145*, 43−57.

(10) McIntyre, R. S., Lophaven, S., and Olsen, C. K. (2014) A randomized, double-blind, placebo-controlled study of vortioxetine on cognitive function in depressed adults. *Int. J. Neuropsychopharmacol. 17*, 1557−1567.

(11) Mahableshwarkar, A. R., Zajecka, J., Jacobson, W., Chen, Y., and Keefe, R. S. (2015) A randomized, placebo-controlled, active-reference, double-blind, flexible-dose study of the efficacy of vortioxetine on cognitive function in major depressive disorder. *Neuropsychopharmacology 40*, 2025−2037.

(12) Pramod, A. B., Foster, J., Carvelli, L., and Henry, L. K. (2013) SLC6 transporters: structure, function, regulation, disease association and therapeutics. *Mol. Aspects Med. 34*, 197−219.

(13) Krishnamurthy, H., and Gouaux, E. (2012) X-ray structures of LeuT in substrate-free outward-open and apo inward-open states. *Nature 481*, 469−474.

(14) Malinauskaite, L., Quick, M., Reinhard, L., Lyons, J. A., Yano, H., Javitch, J. A., and Nissen, P. (2014) A mechanism for intracellular release of Na^+ by neurotransmitter/sodium symporters. *Nat. Struct. Mol. Biol. 21*, 1006−1012.

(15) Penmatsa, A., Wang, K. H., and Gouaux, E. (2013) X-ray structure of dopamine transporter elucidates antidepressant mechanism. *Nature 503*, 85−90.

(16) Wang, K. H., Penmatsa, A., and Gouaux, E. (2015) Neurotransmitter and psychostimulant recognition by the dopamine transporter. *Nature 521*, 322−327.

(17) Penmatsa, A., Wang, K. H., and Gouaux, E. (2015) X-ray structures of Drosophila dopamine transporter in complex with nisoxetine and reboxetine. *Nat. Struct. Mol. Biol. 22*, 506−508.

(18) Yamashita, A., Singh, S. K., Kawate, T., Jin, Y., and Gouaux, E. (2005) Crystal structure of a bacterial homologue of Na^+/Cl^--dependent neurotransmitter transporters. *Nature 437*, 215−223.

(19) Andersen, J., Olsen, L., Hansen, K. B., Taboureau, O., Jørgensen, F. S., Jørgensen, A. M., Bang-Andersen, B., Egebjerg, J., Strømgaard, K., and Kristensen, A. S. (2010) Mutational mapping and modeling of the binding site for (*S*)-citalopram in the human serotonin transporter. *J. Biol. Chem. 285*, 2051−2063.

(20) Andersen, J., Stuhr-Hansen, N., Zachariassen, L. G., Koldsø, H., Schiøtt, B., Strømgaard, K., and Kristensen, A. S. (2014) Molecular basis for selective serotonin reuptake inhibition by the antidepressant agent fluoxetine (Prozac). *Mol. Pharmacol. 85*, 703−714.

(21) Celik, L., Sinning, S., Severinsen, K., Hansen, C. G., Møller, M. S., Bols, M., Wiborg, O., and Schiøtt, B. (2008) Binding of serotonin to the human serotonin transporter. Molecular modeling and experimental validation. *J. Am. Chem. Soc. 130*, 3853−3865.

(22) Forrest, L. R., Zhang, Y. W., Jacobs, M. T., Gesmonde, J., Xie, L., Honig, B. H., and Rudnick, G. (2008) Mechanism for alternating access in neurotransmitter transporters. *Proc. Natl. Acad. Sci. U. S. A. 105*, 10338−10343.

(23) Koldsø, H., Autzen, H. E., Grouleff, J., and Schiøtt, B. (2013) Ligand induced conformational changes of the human serotonin transporter revealed by molecular dynamics simulations. *PLoS One 8*, e63635.

(24) Koldsø, H., Severinsen, K., Tran, T. T., Celik, L., Jensen, H. H., Wiborg, O., Schiøtt, B., and Sinning, S. (2010) The two enantiomers of citalopram bind to the human serotonin transporter in reversed orientations. *J. Am. Chem. Soc. 132*, 1311−1322.

(25) Sinning, S., Musgaard, M., Jensen, M., Severinsen, K., Celik, L., Koldsø, H., Meyer, T., Bols, M., Jensen, H. H., Schiøtt, B., and Wiborg, O. (2010) Binding and orientation of tricyclic antidepressants within the central substrate site of the human serotonin transporter. *J. Biol. Chem. 285*, 8363−8374.

(26) Koldsø, H., Noer, P., Grouleff, J., Autzen, H. E., Sinning, S., and Schiøtt, B. (2011) Unbiased simulations reveal the inward-facing conformation of the human serotonin transporter and Na^+ ion release. *PLoS Comput. Biol. 7*, e1002246.

(27) Piscitelli, C. L., Krishnamurthy, H., and Gouaux, E. (2010) Neurotransmitter/sodium symporter orthologue LeuT has a single high-affinity substrate site. *Nature 468*, 1129−1132.

(28) Singh, S. K., Yamashita, A., and Gouaux, E. (2007) Antidepressant binding site in a bacterial homologue of neurotransmitter transporters. *Nature 448*, 952−956.

(29) Zhou, Z., Zhen, J., Karpowich, N. K., Goetz, R. M., Law, C. J., Reith, M. E., and Wang, D. N. (2007) LeuT-desipramine structure reveals how antidepressants block neurotransmitter reuptake. *Science 317*, 1390−1393.

(30) Zhou, Z., Zhen, J., Karpowich, N. K., Law, C. J., Reith, M. E., and Wang, D. N. (2009) Antidepressant specificity of serotonin transporter suggested by three LeuT-SSRI structures. *Nat. Struct. Mol. Biol. 16*, 652−657.

(31) Wang, H., Goehring, A., Wang, K. H., Penmatsa, A., Ressler, R., and Gouaux, E. (2013) Structural basis for action by diverse antidepressants on biogenic amine transporters. *Nature 503*, 141−145.

(32) Andersen, J., Taboureau, O., Hansen, K. B., Olsen, L., Egebjerg, J., Strømgaard, K., and Kristensen, A. S. (2009) Location of the antidepressant binding site in the serotonin transporter: importance of Ser-438 in recognition of citalopram and tricyclic antidepressants. *J. Biol. Chem. 284*, 10276−10284.

(33) Barker, E. L., Moore, K. R., Rakhshan, F., and Blakely, R. D. (1999) Transmembrane domain I contributes to the permeation pathway for serotonin and ions in the serotonin transporter. *J. Neurosci. 19*, 4705−4717.

(34) Henry, L. K., Field, J. R., Adkins, E. M., Parnas, M. L., Vaughan, R. A., Zou, M. F., Newman, A. H., and Blakely, R. D. (2006) Tyr-95 and Ile-172 in transmembrane segments 1 and 3 of human serotonin

DOI: 10.1021/acschemneuro.5b00225
ACS Chem. Neurosci. 2015, 6, 1892−1900

transporters interact to establish high affinity recognition of antidepressants. *J. Biol. Chem. 281*, 2012−2023.
(35) Sørensen, L., Andersen, J., Thomsen, M., Hansen, S. M., Zhao, X., Sandelin, A., Strømgaard, K., and Kristensen, A. S. (2012) Interaction of antidepressants with the serotonin and norepinephrine transporters: mutational studies of the S1 substrate binding pocket. *J. Biol. Chem. 287*, 43694−43707.
(36) Koldsø, H., Christiansen, A. B., Sinning, S., and Schiøtt, B. (2013) Comparative modeling of the human monoamine transporters: similarities in substrate binding. *ACS Chem. Neurosci. 4*, 295−309.
(37) Stamm, M., Staritzbichler, R., Khafizov, K., and Forrest, L. R. (2014) AlignMe-a membrane protein sequence alignment web server. *Nucleic Acids Res. 42*, W246−W251.
(38) Stamm, M., Staritzbichler, R., Khafizov, K., and Forrest, L. R. (2013) Alignment of helical membrane protein sequences using AlignMe. *PLoS One 8*, e57731.
(39) Khafizov, K., Staritzbichler, R., Stamm, M., and Forrest, L. R. (2010) A study of the evolution of inverted-topology repeats from LeuT-fold transporters using AlignMe. *Biochemistry 49*, 10702−10713.
(40) Braberg, H., Webb, B. M., Tjioe, E., Pieper, U., Sali, A., and Madhusudhan, M. S. (2012) SALIGN: a web server for alignment of multiple protein sequences and structures. *Bioinformatics 28*, 2072−2073.
(41) Eswar, N., Webb, B., Marti-Renom, M. A., Madhusudhan, M. S., Eramian, D., Shen, M. Y., Pieper, U., and Sali, A. (2006) Comparative protein structure modeling using Modeller. *Curr. Protoc. Protein Sci. 50*, 2.9.1−2.9.31.
(42) Sali, A., and Blundell, T. L. (1993) Comparative protein modeling by satisfaction of spatial restraints. *J. Mol. Biol. 234*, 779−815.
(43) Marti-Renom, M. A., Stuart, A. C., Fiser, A., Sanchez, R., Melo, F., and Sali, A. (2000) Comparative protein structure modeling of genes and genomes. *Annu. Rev. Biophys. Biomol. Struct. 29*, 291−325.
(44) Fiser, A., Do, R. K. G., and Sali, A. (2000) Modeling of loops in protein structures. *Protein Sci. 9*, 1753−1773.
(45) Barker, E. L., Perlman, M. A., Adkins, E. M., Houlihan, W. J., Pristupa, Z. B., Niznik, H. B., and Blakely, R. D. (1998) High affinity recognition of serotonin transporter antagonists defined by species-scanning mutagenesis. An aromatic residue in transmembrane domain I dictates species-selective recognition of citalopram and mazindol. *J. Biol. Chem. 273*, 19459−19468.
(46) Sarker, S., Weissensteiner, R., Steiner, I., Sitte, H. H., Ecker, G. F., Freissmuth, M., and Sucic, S. (2010) The high-affinity binding site for tricyclic antidepressants resides in the outer vestibule of the serotonin transporter. *Mol. Pharmacol. 78*, 1026−1035.
(47) Walline, C. C., Nichols, D. E., Carroll, F. I., and Barker, E. L. (2008) Comparative molecular field analysis using selectivity fields reveals residues in the third transmembrane helix of the serotonin transporter associated with substrate and antagonist recognition. *J. Pharmacol. Exp. Ther. 325*, 791−800.
(48) Wacker, D., Wang, C., Katritch, V., Han, G. W., Huang, X. P., Vardy, E., McCorvy, J. D., Jiang, Y., Chu, M., Siu, F. Y., Liu, W., Xu, H. E., Cherezov, V., Roth, B. L., and Stevens, R. C. (2013) Structural features for functional selectivity at serotonin receptors. *Science 340*, 615−619.
(49) Wang, C., Jiang, Y., Ma, J., Wu, H., Wacker, D., Katritch, V., Han, G. W., Liu, W., Huang, X. P., Vardy, E., McCorvy, J. D., Gao, X., Zhou, X. E., Melcher, K., Zhang, C., Bai, F., Yang, H., Yang, L., Jiang, H., Roth, B. L., Cherezov, V., Stevens, R. C., and Xu, H. E. (2013) Structural basis for molecular recognition at serotonin receptors. *Science 340*, 610−614.
(50) Hassaine, G., Deluz, C., Grasso, L., Wyss, R., Tol, M. B., Hovius, R., Graff, A., Stahlberg, H., Tomizaki, T., Desmyter, A., Moreau, C., Li, X. D., Poitevin, F., Vogel, H., and Nury, H. (2014) X-ray structure of the mouse serotonin 5-HT_3 receptor. *Nature 512*, 276−281.

NOTE ADDED AFTER ASAP PUBLICATION

This paper was published on the Web on October 11, 2015, with errors in Figure 5. The corrected version was reposted on October 21, 2015.

DOI: 10.1021/acschemneuro.5b00225
ACS Chem. Neurosci. 2015, 6, 1892−1900